Perovskite Solar Cells with Versatile Electropolymerized Fullerene as Electron Extraction Layer

María B. Suárez[a], Clara Aranda[b], Daniel Heredia[a], Edgardo N. Durantini[a], Luis Otero[a], Miguel Gervaldo[a]*, Antonio Guerrero[b]*

[a] *Departamento de Química, Universidad Nacional de Río Cuarto. Agencia Postal Nro. 3, X5804BYA Río Cuarto, Córdoba, Argentina.*

[b] *Institute of Advanced Materials (INAM), Universitat Jaume I, 12006 Castelló, Spain.*

*****Corresponding Authors

e-mail: mgervaldo@exa.unrc.edu.ar. aguerrer@uji.es

ABSTRACT:

Fullerenes are efficient electron extraction materials (ETL) in perovskite solar cells typically deposited by methods that are non-scalable (i.e. spin coating) or expensive (i.e. vacuum evaporation). In this work we electropolymerize films of a simple 3,4-ethylenedioxythiophene-C_{60} fullerene monomer as scalable and inexpensive alternative process. The technique enables the robust formation of organic layers with a precise thickness control avoiding the use of high temperatures (i.e. TiO_2 requires temperatures >450 °C). The electropolymerized films are highly homogenous, conformal with the FTO substrate and insoluble avoiding undesired dissolution. Electropolymerization of this simple monomer as ETL shows promising efficiencies of 11.0 % after 13 days under operation conditions. The efficiency increases with time and/or by light soaking clearly pointing to increased stability in comparison to the use of discrete fullerenes. The structural versatility of this type of monomers opens a promising avenue for further improvement by chemical modification.

TOC GRAPHICS

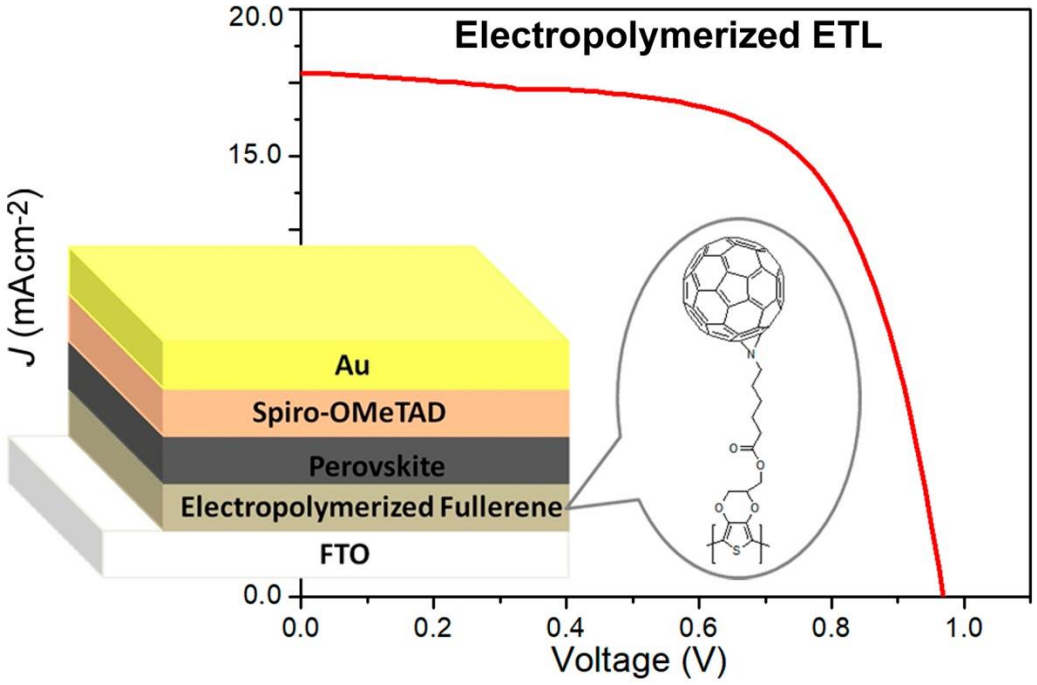

Solar cells based on hybrid organic-inorganic materials with perovskite crystallographic structure have attracted extensive attention that has exponentially grown since their first introduction in 2009.[1-] The "new wave" of this emerging technology has been propelled by the promise of efficient and cost-effective solar energy conversion devices.[4] Perovskite solar cells can be classified into mesoscopic (MHJ) and planar heterojunction (PHJ) configurations.[6] In MHJ devices the perovskite is formed onto a scaffold prepared under high temperature conditions, usually above 450 °C, composed typically by nanostructured titanium, aluminum or zinc oxide.[6] On the contrary, in the PHJ configuration the metal-halide perovskite active layer is sandwiched between two planar charge selective contacts.[78] In this respect, for the development of efficient and stable devices the hole extraction/transport layers (HTL) and the electron extraction/transport layers (ETL) need to fulfill a range of stringent requirements.[9] In general, PHJ solar cells are less efficient than the mesoscopic counterpart but efficiencies are approaching those of MHJ. On the other hand, the PHJ configuration simplifies the fabrication process compared to MHJ avoiding the use of a high temperature step for the sintering of the mesoporous metal oxides enabling the fabrication of large area and flexible perovskite solar cells.[10]

Buckminsterfullerene derivatives with chemical structures derived from those used in organic solar cells have demonstrated to be efficient ETL in planar and mesoscopic perovskite solar cells. [1112-14] In this sense, C_{60} fullerene has shown to be a strong electron acceptor useful not only as selective contact, but also as passivation agent for the charge traps at the grain boundaries of perovskite surface.[15,16] The material is typically deposited as thin layer of about 20-50 nm by spin coating either on the top of the perovskite or onto a transparent conductive substrate. Unfortunately, spin coating is not compatible with industrial processes and alternative cost effective methods are required that accounts for thickness control and high reproducibility. In addition, in many reports the fullerene is used in combination with an metal oxide ETL, not

avoiding the use of high temperature steps or reducing the photodegradation associated to the metal oxide.[17,18] Discrete fullerenes can be dissolved during processing of the subsequent layers. Wojciechowski *et al.*[14] showed that insoluble films could be obtained by the use of cross-linking units improving the n-type charge collection contact with efficiencies in the range of 12-16 %. However, spin coating was still needed for deposition of fullerene and crosslinker. More importantly, discrete fullerene materials frequently suffer from aggregation during the lifetime of the device as observed in organic photovoltaic devices affecting the long term device stability.[19] Thus, development of PHJ solar cells using fullerene based selective contacts is required to go through alternative methods to spin coating whilst obtaining adequate efficiency and stability of the devices.

Recently, Yan *et al.* [2021] demonstrated the use of electropolymerized organic films as HTLs in inverted perovskite solar cells with efficiencies in the range of 12-16 %. Electrochemical synthesis enables generation of polymers with high uniformity, high stability, and well-controlled thickness.[22,23] In addition, the methodology is scalable at low-cost and does not produce large amounts of pollutant solvent waste. For these reasons in the present report we extend the use of electrochemical deposition of polymeric films at low temperatures for the production of ETLs by using a monomer composed by 3,4-ethylenedioxythiophene (EDOT) units containing C_{60} pendant moieties (Figure 1a). Solar cells fabricated with this simple monomer show remarkable stabilized efficiencies of 11.0 % after 13 days under operation conditions.

The polymer containing C_{60} units (Figure 1b) was generated over FTO electrodes in one single step by cyclic voltammetry in the range of -0.50 to 1.30 V vs SCE, see supporting information for details. Thickness control of the ETL layer was obtained by modifying the number of polymerization cycles. i.e. 5 polymerization cycles lead to 20 nm. The electrical

properties of electropolymerized films were also characterized by cyclic voltammetry in a dichloromethane solution only containing supporting electrolyte (Figure 2a). The electrical response of the PEDOT-C_{60} film as a function of the scan rate is very different to the response reported for PEDOT, where a large capacitive current is observed in the -0.4 to 1.0 V range. PEDOT-C_{60} shows one anodic peak at around 1.2 V, one very sharp peak at -0.46 V, and two bell shaped cathodic peaks at -0.71 and -1.18 V (Figure 2a). The peak currents present a lineal relation with the scan rate, typical of an electroactive product irreversibly adsorbed on the electrode surface. The cathodic peaks at -0.71 and -1.18 V are assigned to first and second reduction of the C_{60} units, while the anodic peak is attributed to oxidation of the PEDOT units. The observed cathodic peaks confirm that the C_{60} units are still present in the film after the electropolymerization process, and retains its electrochemical properties. By using the oxidation and reduction redox potentials the polymer HOMO and LUMO levels are estimated at energies of -5.98 and -4.09 eV, respectively.[24]

The transmission spectra of PEDOT-C_{60} films (Figure 2b) show that the films are highly transparent with bands at 330, 390, 470, and 630 nm. The intensity of all bands increases with the number of polymerization cycles, indicating that the films become thicker with every new polymerization cycle. These bands are assigned to electronic transitions due to the presence of C_{60} aggregates in the films, as it has been previously reported for C_{60} layers deposited by physical vapor deposition.[25-27] Taking into account the electrochemical and spectroscopic data, a polymer structure where the fullerenes units are pending from the PEDOT principal chain is proposed (Figure 1b). Stacks containing FTO/ PEDOT-C_{60}/perovskite show transmission close to 0 in the range 300-800 nm (Figure 2b) due to the absorbance of the $CH_3NH_3PbI_3$ films, with an on-set at 792 nm (1.56 eV). Figure 2c shows the energy diagram of the device, the correct

alignment of the perovskite conduction band with the PEDOT-C_{60} LUMO makes possible the electron transfer process from the perovskite to the PEDOT-C_{60} layer.

A back-scattering cross-section scanning electron microscopy (SEM) image of the complete device is shown in Figure 3a for a device fabricated with five polymerization cycles of PEDOT-C_{60}. A thickness of about 20 nm is estimated for the PEDOT-C_{60} layer as observed by the dark conformal layer present on the top of the FTO layer. It is observed that the perovskite deposits uniformly on the top of the PEDOT-C_{60} layer leading to adequate morphologies. Atomic Force Microscopy analysis (Figure 3b) shows that the PEDOT-C_{60} film is free of pinholes and homogenous, and follows the topography of the FTO layer (see supporting information). The roughness of the film is very low (RMS=3-5 nm), similar to those observed for PEDOT:PSS films.

Regarding the *J-V* response, Figure 4a shows the illumination effect on the performance of a solar cell device with a PEDOT-C_{60} layer obtained by one polymerization cycle. Devices are measured under reverse bias at a low 50 mV/s scan rate to minimize the effect of hysteresis which is still observed. Before light exposure fresh devices presents very low performance with the following photovoltaic parameters: open circuit potential (V_{oc}) of 554 mV, short circuit current (J_{sc}) of 13.7 mA/cm^2 and Fill Factor (*FF*) of 43 %, and power conversion efficiency (PCE) of 3.3%. Interestingly, the performance of the device progressively increases with the illumination time until all the photovoltaic parameters reach almost constant values after five minutes. During this period of time the V_{oc} and the *FF* are the two parameters most affected increasing the PCE to 8.0 % (V_{oc}= 875 mV, J_{sc}=14.54 mA/cm^2, FF= 62.7). The results above clearly show that activation of the ETL is required by light soaking treatment leading to important improvement of the performance with illumination. This effect has been observed previously for some perovskite devices and has been attributed to different causes which may not

be related to our case of study due to novelty of our new system. For example, Shao et al. reported the use of a fullerene derivative with a high dielectric constant which suppressed both, the trap assisted recombination at interface between the perovskite and the C_{60}, and the light soaking effect.[28] It has also been proposed by Zhao et al. that the photogenerated charges neutralize the charges localized at the electrode interface, increasing the V_{oc} and FF.[29] In both studies they used an inverted configuration and the C_{60} layer was spin coated over the perovskite. The surface traps in TiO_2 electron transport layer have also been the cause of the light soaking.[30,31] In our system this layer is not present and we propose that during the light soaking experiments ions are penetrating into the organic layer increasing the conductivity of the layer and reducing its resistance and recombination processes. This would be in good agreement with different proves that suggest that iodine ions migrate to the contacts under the effect of light and applied bias.[32-34] Further studies to clarify the mechanism in which light soaking modifies the device performance are required but these are beyond the scope of this work.

The effect of the light soaking and stability was studied as a function of the PEDOT-C_{60} layer thickness as shown in the supporting information. A marked relationship between thickness of PEDOT-C_{60} layer and efficiency evolution is not observed but the J_{sc} and PCE slowly increases with the time and after thirteen days the PCE is still increasing. The lack of a trend is probably related with the variability of kinetics in ions penetrating into the PEDOT-C_{60} layer but in any case the results clearly demonstrate that devices present adequate stability with the time. Figure 4b shows stabilized efficiency of representative devices after 13 days as a function of the number of polymerization cycles of PEDOT-C_{60} layer. Performance of the devices increases with the number of cycles up to 2 cycles leading to PCE values of 11.0 %. Then, as the thickness is further increased the efficiency decreases with lowest values for 5 polymerization cycles. We attribute these results to the low conductivity of the material that requires very thin layers.

Importantly, cells without the PEDOT-C_{60} typically lead to devices with very low efficiency (average values of ~3 % out of 80 samples). Therefore, the beneficial effect of the PEDOT-C_{60} layer as electron transport layer in perovskite solar cells is demonstrated. Further improvements in the ETL are possible by further optimization the deposition conditions like monomer concentration, support electrolyte or electrochemical deposition method. In addition, modification in the monomers structure is simple and may lead to significant efficiency improvements.

In summary, a new C_{60} derivative monomer was electropolymerized on FTO electrodes and used as a ETM in perovskite solar cells using a method that is compatible with industrial requirements. The PEDOT-C_{60} electropolymer was easily obtained by a simple electrochemical methodology in one single step, avoiding the use of high temperatures which are employed in the formation of TiO_2 layers. Films are very smooth, conformal with the FTO substrate, highly transparent and are obtained with accurate thickness control. The devices constructed with the PEDOT-C_{60} electropolymer showed light soaking effects, reaching constant photovoltaic parameters after five illumination minutes. Measurements carried as a function of the time showed that the efficiency evolves with time increasing with nearly stable values after thirteen days. Best devices show a promising efficiency of 11.0%. Further improvements in the ETL are foreseen by further optimization of the layer and by modification in the monomers structure. The use of a simple electrochemical methodology in the formation of organic electron transport layers as replacement of metal oxides in perovskite solar cells using low temperature conditions opens a new approach in the fabrication of efficient energy conversion systems.

AUTHOR INFORMATION

Corresponding Authors

*Tel.: 54-(0)358-4676195. Fax: 54-(0)358-4676233. E-mail: mgervaldo@exa.unrc.edu.ar.

*Tel.: +34 964 387 555. Fax: +34964387322. E-mail: aguerrer@uji.es.

ACKNOWLEDGMENTS

Authors are grateful to Secretaría de Ciencia y Técnica, Universidad Nacional de Río Cuarto (Secyt-UNRC), Consejo Nacional de Investigaciones Científicas y Técnicas (CONICET) and Agencia Nacional de Promoción Científica y Tecnológica (ANPCYT) of Argentina for financial support. D.H., L.O., and M.G., are Scientific Members of CONICET. M.B.S. thanks to CONICET, for postdoctoral fellowship. C.A. and A.G. thank financial support by MINECO of Spain under project (MAT2016-76892-C3-1-R, RYC-2014-16809) and Generalitad Valenciana (PROMETEOII/2014/020).

REFERENCES

(1) Kojima, A.; Teshima, K.; Shirai, Y.; Miyasaka, T. Organometal Halide Perovskites as Visible-Light Sensitizers for Photovoltaic Cells. *J. Am. Chem. Soc.* **2009**, *131*, 6050-6051.

(2) Bi, D.; Tress, W.; Dar, M.I.; Gao, P.; Luo, J.; Renevier, C.; Schenk, K.; Abate, A.; Giordano, F.; Baena, J.-P. C. Efficient Luminescent Solar Cells Based on Tailored Mixed-Cation Perovskites. *Sci. Adv.* **2016**, *2*, e1501170.

(3) Yang, W. S.; Noh, J. H.; Jeon, N. J.; Kim, Y. C.; Ryu, S.; Seo, J.; Seok, S. I. High-Performance Photovoltaic Perovskite Layers Fabricated Through Intramolecular Exchange. *Science*. **2015**, *348*, 1234-1237.

(4) De Angelis, F.; Kamat, P. V. Riding The New Wave of Perovskites. *ACS Energy Lett.* **2017**, *2*, 922-923.

(5) Lee, M.M.; Teuscher, J.; Miyasaka, T.; Murakami, T.N.; Snaith, H.J. Efficient Hybrid Solar Cells Based on Meso-Superstructured Organometal Halide Perovskites. *Science.* **2012**, *338*, 643-

647.

(6) Ke, W.; Fang, G.; Liu, Q.; Xiong, L.; Qin, P.; Tao, H.; Wang, J.; Lei, H.; Li, B.; Wan, J. Low-Temperature Solution-Processed Tin Oxide as an Alternative Electron Transporting Layer for Efficient Perovskite Solar Cells. *J. Am. Chem. Soc.* **2015**, *137*, 6730-6733.

(7) Liu, D.; Kelly, T.L. Perovskite Solar Cells with w Planar Heterojunction Structure Prepared Using Room-Temperature Solution Processing Techniques. *Nat. Photonics.* **2013**, *8*, 133-138.

(8) Jeng, J.Y.; Chiang, Y.F.; Lee, M.H.; Peng, S.R.; Guo, T.F.; Chen, P.; Wen, T.C. CH3NH3PbI3 Perovskite/Fullerene Planar-Heterojunction Hybrid Solar Cells. *Adv. Mater.* **2013**, *25*, 3727-3732.

(9) Yin, W.; Pan, L.; Yang, T.; Liang, Y. Recent Advances in Interface Engineering for Planar Heterojunction Perovskite Solar Cells. *Molecules.* **2016**, 21(7), 837.

(10) You, J.; Hong, Z.; Yang, Y. (Michael); Chen, Q.; Cai, M.; Song, T-B.; Chen, C-C.; Lu, S.; Liu, Y.; Zhou, H.; Yang, Y. Low-Temperature Solution-Processed Perovskite Solar Cells with High Efficiency and Flexibility. *ACS Nano.* **2014**, *8*,1674-1680.

(11) Fang, Y.; Bi, C.; Wang, D.; Huang, J. The Functions of Fullerenes in Hybrid Perovskite Solar Cells. *ACS Energy Lett.* **2017**, *2*, 782-794.

(12) Li, Y.; Zhao, Y.; Chen, Q.; Yang, Y.; Liu, Y.; Hong, Z.; Liu, Z.; Hsieh, Y.-T.; Meng, L.; Li, Y. Multifunctional Fullerene Derivative for Interface Engineering in Perovskite Solar Cells. *J. Am. Chem. Soc.* **2015**, *137*, 15540-15547.

(13) Liu, C.; Wang, K.; Du, P.; Meng, T.; Yu, X.; Cheng, Stephen Z. D.; Gong, X. High Performance Planar Heterojunction Perovskite Solar Cells with Fullerene Derivatives as the Electron Transport Layer. *ACS Appl. Mater. Interfaces.* **2015**, *7*, 1153-1159

(14) Wojciechowski, K.; Ramirez, I.; Gorisse, T.; Dautel, O.; Dasari, R.; Sakai, N.; Martinez Hardigree, J.; Song, S.; Marder, S.; Riede, M.; Wantz, G.; Snaith H.J. Cross-Linkable Fullerene Derivatives for Solution-Processed n–i–p Perovskite Solar Cells. *ACS Energy Lett.* **2016**, *1*, 648-653.

(15) Valles-Pelarda, M.; Clasen Hames, B.; García-Benito, I.; Almora, O.; Molina-Ontoria, A.;. Sánchez, R. S.; Garcia-Belmonte, G.; Martín, N.; Mora-Sero, I. Analysis of the Hysteresis Behavior of Perovskite Solar Cells with Interfacial Fullerene Self-Assembled Monolayers. *J. Phys. Chem. Lett.* **2016**, *7*, 4622-4628

(16) Shao, Y.; Xiao, Z.; Bi, C.; Yuan, Y.; Huang, J. Origin and Elimination of Photocurrent Hysteresis by Fullerene Passivation in CH3NH3PbI3 Planar Heterojunction Solar Cells. *Nat. Commun.* **2014,** *5*, 5784.

(17) Tao, C.; Neutzner, S.; Colella, L.; Marras, S.; Srimath Kandada, A. R.; Gandini, M.; Bastiani, M. D.; Pace, G.; Manna, L.; Caironi, M. 17.6% Stabilized Efficiency in Low-Temperature Processed Planar Perovskite Solar Cells. *Energy Environ. Sci.* **2015**, *8*, 2365-2370.

(18) Zhong, Y.; Munir, R.; Balawi, A.H.; Sheikh, A. D.; Yu, L.; Tang, M.-C.; Hu, H.; Laquai, F.; Amassian, A. Mesostructured Fullerene Electrodes for Highly Efficient n−i−p Perovskite Solar Cells. *ACS Energy Lett*. **2016**, *1*, 1049-1056.

(19) Guerrero, A.; Garcia-Belmonte, G. Recent Advances to Understand Morphology Stability of Organic Photovoltaics. *Nano-Micro Letters.* **2016**, 9 (1), 10.

(20) Yan, W.; Li, Y.; Li, Y.; Ye, S.; Liu, Z.; Wang, S.; Bian, Z.; Huang, C. High-Performance Hybrid Perovskite Solar Cells with Open Circuit Voltage Dependence on Hole-Transporting Materials. *Nano Energy.* **2015**, *16*, 428-437.

(21) Yan, W.; Li, Y.; Li, Y.; Ye, S.; Liu, Z.; Wang, S.; Bian, Z.; Huang, C. Stable High-Performance Hybrid Perovskite Solar Cells with Ultrathin Polythiophene as Hole-Transporting Layer. *Nano Res*. **2015**, *8*, 2474.

(22) Solis, C.; Ballatore, M.B.; Suarez, M.B.; Milanesio, M.E.; Durantini, E.N.; Santo, M.; Dittrich, Th.; Otero, L.; Gervaldo, M. Electrochemical Generation of a Molecular Heterojunction. A New Zn-Porphyrin-Fullerene C60 Polymeric Film. *Electrochim. Acta.*, **2017**, *238*, 81-90.

(23) Gervaldo, M.; Liddell, P.A.; Kodis, G.; Brennan, B.J.; Johnson, C.R.; Bridgewater, J.W.; Moore, A.L.; Moore, T.A.; Gust, D. A Photo- and Electrochemically-Active Porphyrin-Fullerene Dyad Electropolymer. *Photochem. Photobiol. Sci.* **2010**, *9*, 890-900.

(24) Ahn, N.; Son, D-Y; Jang, I-H.; Kang, S.M.; Choi, M.; Park, N-G. Highly Reproducible Perovskite Solar Cells with Average Efficiency of 18.3% and Best Efficiency of 19.7% Fabricated via Lewis Base Adduct of Lead(II) Iodide. *J. Am. Chem. Soc.*, **2015**, *137*, 8696-8699.

(25) Fravventura, M.C.; Hwang, J.; Suijkerbuijk, J.W.A.; Erk, P.; Siebbeles, L.D.A.; Savenije, T.J. Determination of Singlet Exciton Diffusion Length in Thin Evaporated C60 Films for Photovoltaics. *J. Phys. Chem. Lett.* **2012**, *3*, 2367-2373.

(26) Capozzi, V.; Casamassima, G.; Lorusso, G. F.; Minafra, A.; Piccolo, R.; Trovato, T.; Valentini, A. Optical Spectra and Photoluminescence of C60 Thin Films. *Solid State Commun.* **1996**, *98*, 853-858.

(27) Negri, F.; Orlandi, G.; Zerbetto, F. Interpretation of the Vibrational Structure of the Emission and Absorption Spectra of C60. *J. Chem. Phys.* **1992**, *97*, 6496-6503.

(28) Shao, S.; Abdu-Aguye, M.; Qiu, L.; Lai, L-H.; Liu, J.; Adjokatse, S.; Jahani, F.; Kamminga, M.E.; Ten Brink, G.H.; Palstra, T.T.M.; Kooi, B.J.; Hummelen, J.C.; Loi, M.A. Elimination of the Light Soaking Effect and Performance Enhancement in Perovskite Solar Cells Using a Fullerene Derivative. *Energy Environ. Sci.* **2016**, *9*, 2444-2452.

(29) Zhao, C.; Chen, B.; Qiao, X.; Luan, L.; Lu, K.; Hu, B. *Adv. Energy Mater*., **2015**, *5*, 1500279.

(30) Li, Y.; Zhao, Y.; Chen, Q.; Yang, Y. (Michael); Liu, Y.; Hong, Z.; Liu, Z.; Hsieh, Y.-T.; Meng, L.; Li, Y.; Yang, Y. Multifunctional Fullerene Derivative for Interface Engineering in Perovskite Solar Cells. *J. Am. Chem. Soc*. **2015**, *137*, 15540-15547.

(31) Heo, J.H.; You, M.S.; Chang, M.H.; Yin, W.; Ahn, T.K.; Lee, S.-J.; Sung, S.-J.; Kim, D.H.; Im, S.H. Hysteresis-less Mesoscopic CH3NH3PbI3 Perovskite Hybrid Solar Cells by Introduction of Li-treated TiO2 Electrode. *Nano Energy.* **2015**, *15*, 530-539.

(32) Gottesman, R.; Lopez-Varo, P.; Gouda, L.; Jimenez-Tejada, Juan A.; Hu, J.; Tirosh, S.; Zaban, A.; Bisquert, J. Dynamic Phenomena at Perovskite/Electron-Selective Contact Interface as Interpreted from Photovoltage Decays. *Chem.* **2016**, *1*, 776-789.

(33) Guerrero, A.; You, J.; Aranda, C.; Kang, Y. S.; Garcia-Belmonte, G.; Zhou, H.; Bisquert, J.; Yang, Y. Interfacial Degradation of Planar Lead Halide Perovskite Solar Cells. *ACS Nano.* **2016**, *10*, 218-224.

(34) Carrillo, J.; Guerrero, A.; Rahimnejad, S.; Almora, O.; Zarazua, I.; Mas-Marza, E.; Bisquert, J.; Garcia-Belmonte, G. Ionic Reactivity at Contacts and Aging of Methylammonium Lead Triiodide Perovskite Solar Cell. *Adv. Energy Mater.* **2016**, *6*, 1502246.

Captions for Figures.

Figure 1: a) Chemical structure of EDOT-C_{60} monomer and b) proposed structure of PEDOT-C_{60} polymer.

Figure 2: a) Cyclic voltammograms at different scan rates of a PEDOT-C_{60} film deposited on FTO electrodes, in a solution containing only a support electrolyte. b) Transmission spectra of electropolymerized films on FTO electrodes (thick lines), and transmission spectra of perovskite films deposited on top of PEDOT-C_{60} polymer (thin lines). c) Proposed energy level diagram by using literature values and those calculated for PEDOT-C_{60} from data in Figure 2a.

Figure 3: a) Back-scattering cross sectional SEM image showing the device architecture. b) Atomic Force Microscopy image of a PEDOT-C_{60} film deposited on a FTO substrate.

Figure 4: Characteristic *J-V* response of devices measured under 1 sun light intensity and at 50 mV/s. a) Fresh device containing one polymerization cycle of PEDOT-C_{60} as a function of the light soaking time and b) Stabilized efficiency after 13 days under storage of devices fabricated with different PEDOT-C_{60} layer thickness by modification of the number polymerization cycles.

Figure 1.

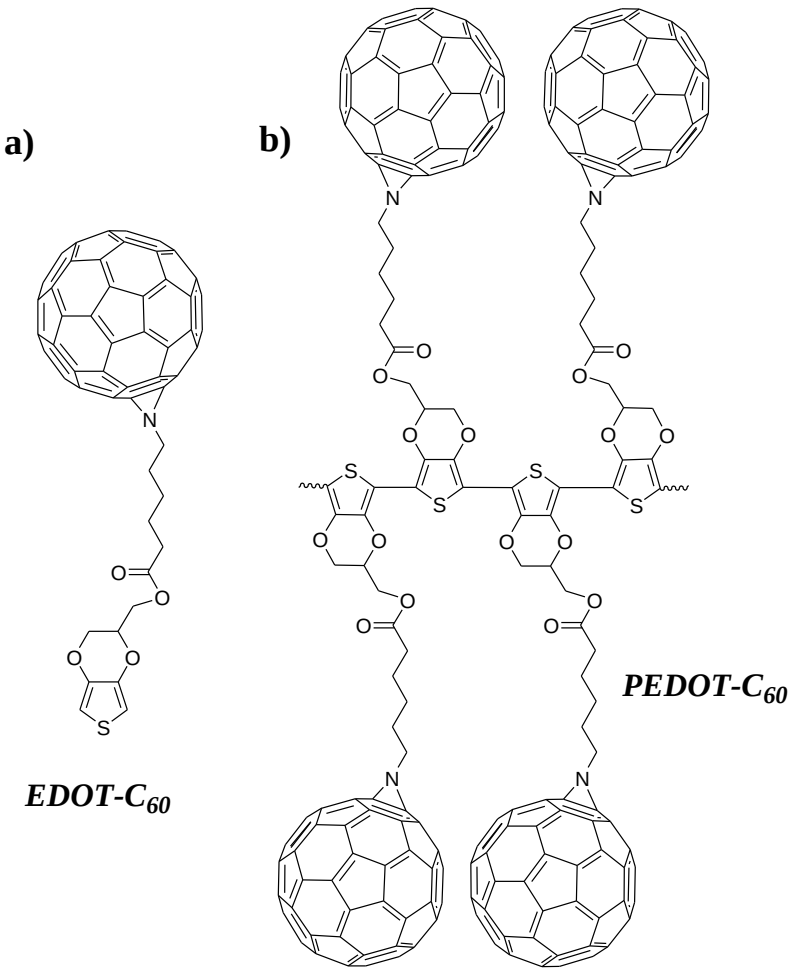

Figure 2.

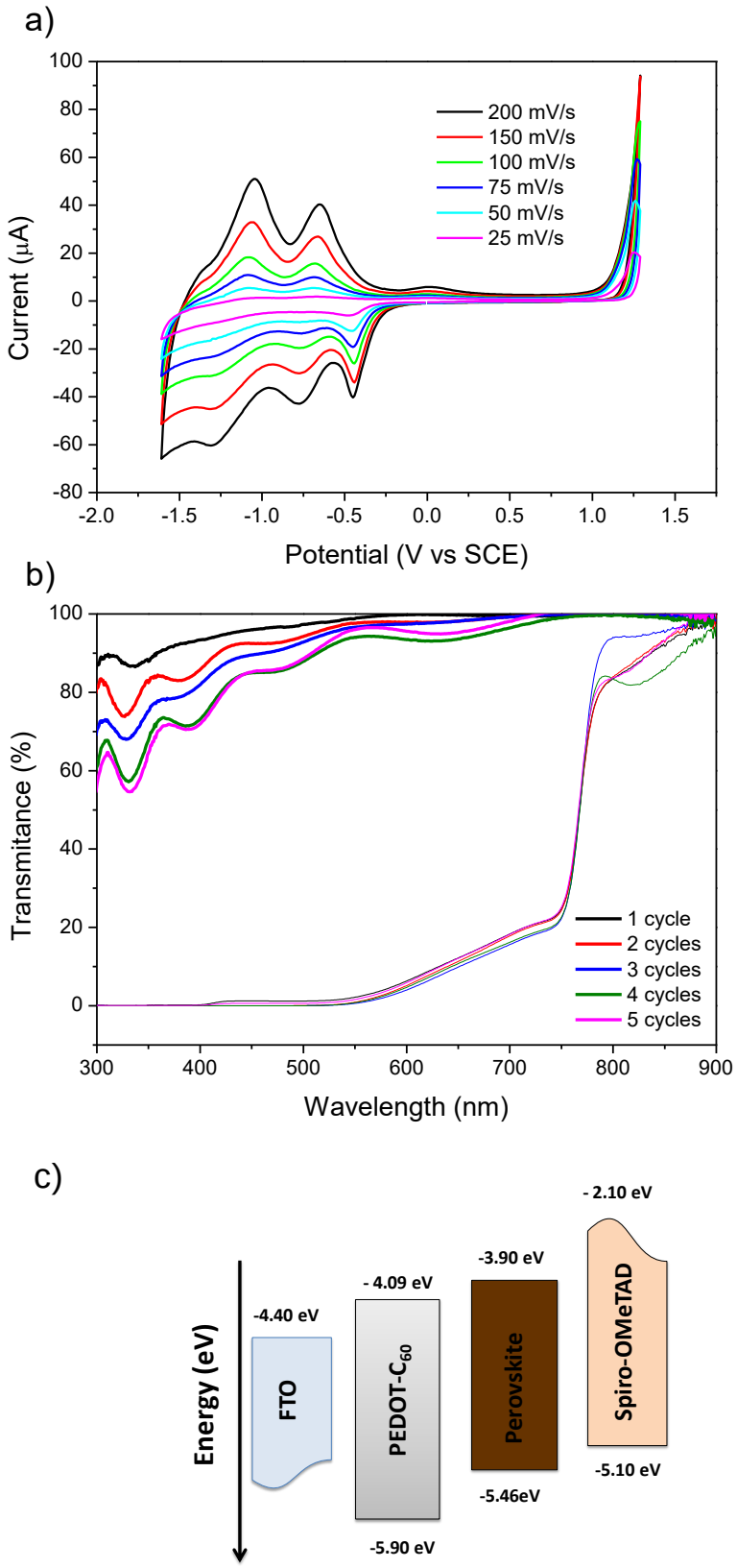
a)
Current (μA)
Potential (V vs SCE)
200 mV/s
150 mV/s
100 mV/s
75 mV/s
50 mV/s
25 mV/s
b)
Transmitance (%)
Wavelength (nm)
1 cycle
2 cycles
3 cycles
4 cycles
5 cycles
c)
Energy (eV)
FTO
-4.40 eV
PEDOT-C60
- 4.09 eV
-5.90 eV
Perovskite
-3.90 eV
-5.46eV
Spiro-OMeTAD
- 2.10 eV
-5.10 eV

Figure 3.

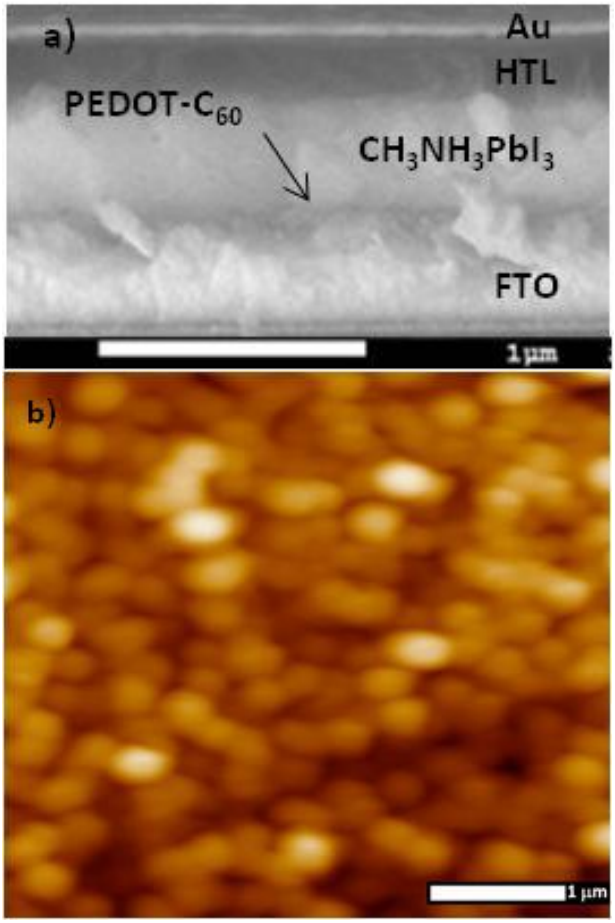

Figure 4

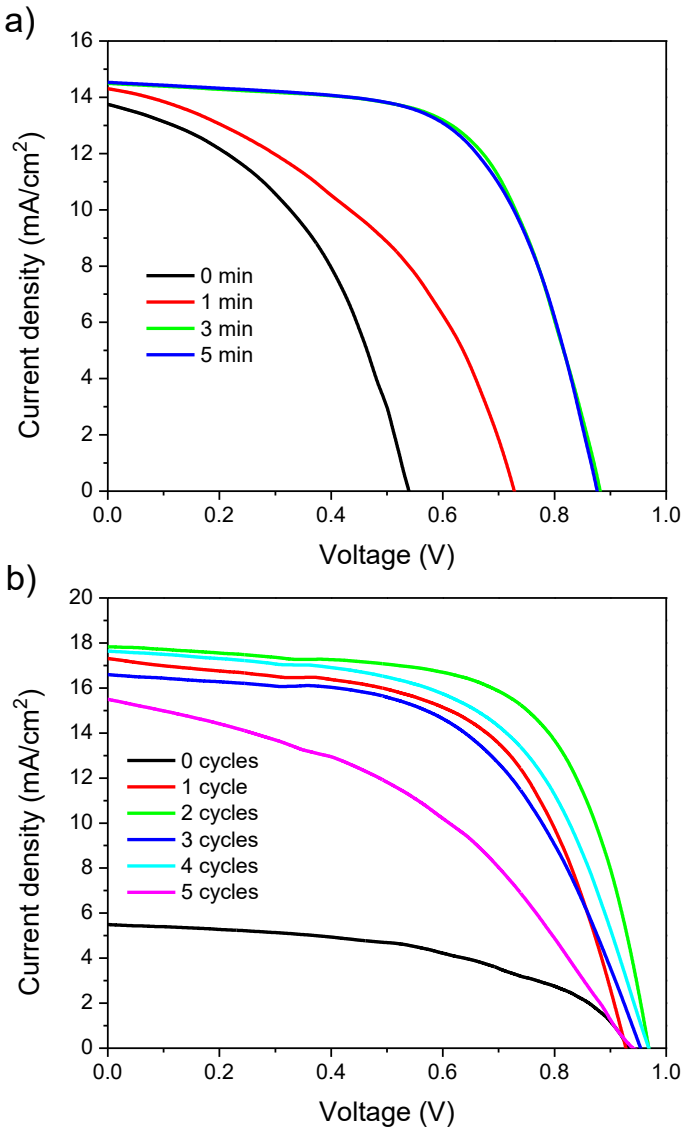
a)
Current density (mA/cm^2)
Voltage (V)
0 min
1 min
3 min
5 min
b)
Current density (mA/cm^2)
Voltage (V)
0 cycles
1 cycle
2 cycles
3 cycles
4 cycles
5 cycles